HHS Public Access

Author manuscript

Nat Struct Mol Biol. Author manuscript; available in PMC 2014 January 01.

Published in final edited form as:

Nat Struct Mol Biol. 2013 July ; 20(7): 781–788. doi:10.1038/nsmb.2616.

Conformational switching of the 26S proteasome enables substrate degradation

Mary E. Matyskiela[1], **Gabriel C. Lander**[2,4], and **Andreas Martin**[1,3]

[1]Department of Molecular and Cell Biology. University of California, Berkeley, California, USA

[2]Life Sciences Division, Lawrence Berkeley National Laboratory, University of California, Berkeley, California, USA

[3]California Institute for Quantitative Biosciences, University of California, Berkeley, California, USA

Abstract

The 26S proteasome is the major eukaryotic ATP-dependent protease, responsible for regulating the proteome through degradation of ubiquitin-tagged substrates. Its regulatory particle, containing the heterohexameric AAA+ ATPase motor and the essential deubiquitinase Rpn11, recognizes substrates, removes their ubiquitin chains, and translocates them into the associated peptidase after unfolding, but detailed mechanisms remain unknown. Here we present the first structure of the 26S proteasome from *S. cerevisiae* during substrate degradation, showing that the regulatory particle switches from a pre-engaged to a translocation-competent conformation. This conformation is characterized by a rearranged ATPase ring with uniform subunit interfaces, a widened central channel coaxially aligned with the peptidase, and a spiral orientation of pore loops that suggests a rapid progression of ATP-hydrolysis events around the ring. Importantly, Rpn11 moves from an occluded position to directly above the central pore, facilitating substrate deubiquitination concomitant with translocation.

Keywords

26S proteasome; 19S regulatory particle; Rpn11; deubiquitination; AAA+ ATPase; protein translocation; cryo-EM; UPS

Correspondence should be addressed to G.C.L. (glander@scripps.edu) and A.M. (a.martin@berkeley.edu).

[4]Present address: The Scripps Research Institute, La Jolla, California, USA

Accession Codes

The cryo-electron microscopy density maps for the mutant 26S proteasomes ($Rpn11^{AXA}$ Rpn13Δ) in the absence and presence of substrate can be found at the Electron Microscopy Data Bank under accession numbers EMD-5668 and EMD-5669, respectively.

Author contributions:

M.E.M. designed, expressed, and purified proteasome constructs, and performed biochemical experiments. G.C.L. performed the electron microcopy, processing, and segmentation analyses. All authors contributed to experimental design, data analyses, and manuscript preparation.

Introduction

The ubiquitin-proteasome system is responsible for rapid degradation of critical regulatory proteins as well as proteome quality control and homeostasis in all eukaryotic cells [1]. Substrates selected for degradation are covalently marked with chains of the small protein ubiquitin, which targets them to the 26S proteasome for subsequent proteolysis. While recent studies have illuminated the overall architecture of this ATP-dependent protease, the structural and molecular mechanisms of substrate engagement and translocation remain poorly understood. Indeed, little is known about the detailed mechanisms of AAA+ (ATPases associated with various cellular activities) protein unfoldases in general, despite the broad importance of ATP-dependent protein unfolding, remodeling, and degradation in the cell [2].

The 26S proteasome is a massive molecular machine with at least 34 different subunits, forming a barrel-shaped 20S peptidase capped on one or both ends by a 19S regulatory particle [3]. The proteolytic active sites of the peptidase are sequestered in an internal chamber, which protein substrates can access only after unfolding, deubiquitination, and translocation by the regulatory particle [4–6]. This regulatory particle consists of 20 subunits and can be divided into two stably associated subcomplexes, the lid and the base [7].

The base subcomplex contains the proteasomal molecular motor, a heterohexameric ring of six distinct AAA+ ATPase subunits in the order Rpt1–Rpt2–Rpt6–Rpt3–Rpt4–Rpt5 [8,9]. In addition, it includes two large scaffolding proteins (Rpn1 and Rpn2), the ubiquitin receptor Rpn13 [10], and the non-essential deubiquitinating enzyme (DUB) Ubp6 [11]. The AAA+ domains of the ATPase subunits are predicted to contact the substrate via conserved loops in the central pore and use the energy of ATP binding and hydrolysis to undergo conformational changes and exert a mechanical pulling force, that unfold and translocate the substrate into the peptidase [12–16]. Each ATPase subunit also contains an N-terminal domain, which is composed of an OB-fold (oligomer binding fold) and an N-terminal helix [17]. Together, the six OB-folds of the ATPase hexamer form a separate ring (the N-ring) above the AAA+ domains, while the N-terminal helices pair into three coiled coils that protrude from this N-ring. Distinct tails at the C-termini of the ATPase subunits mediate attachment of the base to the 20S peptidase through interactions with dedicated pockets on the peptidase surface [18,19]. Previous structural studies have shown that these two subcomplexes bind in an asymmetric fashion, with the AAA+- and N-ring pores surprisingly offset from a coaxial alignment with the peptidase [20–22].

The lid subcomplex is laterally bound to the holoenzyme, partially surrounding the base and also contacting the 20S peptidase [20]. Six of the lid subunits (Rpn3, Rpn5, Rpn6, Rpn7, Rpn9, Rpn12) interact through C-terminal PCI (proteasome-CSN-eIF3) domains in a horseshoe-shaped arrangement, with their N-terminal domains extending radially outward [20,23]. The intrinsic ubiquitin receptor Rpn10 binds to the periphery of the proteasome at the far end of Rpn9's N-terminal domain. Rpn8 and the essential DUB Rpn11 [24] form a dimer that projects toward the center of the regulatory particle [25], positioning Rpn11 near the N-ring. This DUB has been shown to remove entire ubiquitin chains from the substrate by cleaving the isopeptide bond of the proximal ubiquitin

moiety [26]. Interestingly, Rpn11's deubiquitination activity was found to depend on ATP hydrolysis by the proteasome, suggesting a potential coupling with substrate translocation [24]. However, the mechanism for this coupling remains unknown.

Previous crystallographic studies of several related RecA-type and AAA+ helicases revealed that their AAA+ domains and pore loops deviate from a planar organization and exhibit staircase arrangements around the hexameric ring [27–29]. Based on current mechanistic models for these motors, individual AAA+ domains are predicted to continually progress through the distinct conformational registers of the staircase as they hydrolyze ATP [27]. Accordingly, within an ensemble of hydrolyzing proteasome particles, the heterohexameric ATPase ring would be expected to display a variety of distinct conformational states. However, previous EM reconstructions of the proteasome in the presence of saturating ATP show that the ATPase domains adopt a fixed spiral staircase arrangement, with Rpt3 in the highest and Rpt2 in the lowest position for every complex [20,25]. The fixed organization of the proteasomal ATPases thus contradicts the currently predicted mechanisms for AAA+ unfoldases, suggesting that either the observed staircase reflects a translocation-incompetent state or substrate translocation functions by an alternative mechanism. Distinguishing between these scenarios has thus far been impossible due to the lack of structural information on the proteasome or any other protein unfoldase during substrate degradation.

To gain structural insights into the mechanisms of substrate processing by the 26S proteasome, we solved the cryo-EM structure of the holoenzyme during the degradation of an ubiquitin-tagged substrate. We identified an alternative, translocation-competent conformation of the regulatory particle, characterized by a repositioned Rpn11 and a rearranged ATPase ring that together enable efficient substrate degradation.

Results

Structure of substrate-bound proteasome

We first solved the cryo-EM structure of wild-type holoenzyme during degradation of a ubiquitinated substrate. Occupancy was maximized by incubating the proteasome with an excess of a previously characterized model substrate [20], consisting of GFP fused to a destabilized titin I27 domain and an unstructured 111 amino acid segment for engagement [30,31]. 2D analysis revealed that the regulatory particles of these actively degrading proteasomes were much more variable than those of previously observed ATP-bound, substrate-free (apo) proteasomes (Supplementary Figure 1a-c). Three-dimensional analyses showed that a large fraction of the regulatory particles had undergone a dramatic rearrangement, which included a blockage of the N-ring pore by Rpn11 as well as the formation of contacts between Rpn10 and the Rpt4–Rpt5 coiled coil (Figure 1, Supplementary Figure 1d). Notably, the regulatory particles in this altered conformation displayed an additional low-resolution electron density near the N-ring and Rpn11, consistent with a flexibly attached globular structure. GFP exhibits a high thermodynamic stability and fast refolding kinetics [32], and may have numerous ubiquitin chains attached to its many surface-exposed lysine residues. Due to these obstacles, GFP processing may represent the rate-limiting step in the degradation of this substrate, causing an accumulation of proteasome particles that have translocated the fusion construct up to the GFP moiety.

This would suggest that the observed additional density arises from folded GFP at the entrance to the N-ring (Figure 1, Supplementary Figure 1e).

Within the ensemble of doubly-capped proteasomes, we observed three different populations of holoenzyme. 25% showed both regulatory particles in the substrate-engaged conformation, 35% had both regulatory particles in the apo conformation with no indication of additional density, and 40% were asymmetric with one apo and one substrate-engaged regulatory particle. The fact that we observe this distribution of asymmetric as well as dually-translocating proteasomes indicates that there is neither positive nor negative cooperativity between the two regulatory particles of the holoenzyme. Substrate degradation can thus also occur simultaneously from both ends, which had been unexpected based on previous studies of other AAA+ proteases [33].

In order to achieve a higher resolution structure of the regulatory particle in the translocating conformation, it was necessary to trap a uniform ensemble of substrate-engaged proteasome particles. We therefore purified yeast 26S holoenzymes containing an Rpn11 active site mutation (AXA [24,34], Supplementary Figure 2a) that abolishes de-ubiquitination. This mutation prevents further substrate processing when the uncleaved ubiquitin chain arrives at the entrance to the unfoldase pore [24,26]. To additionally increase sample homogeneity, we deleted Rpn13, making Rpn10 the sole intrinsic ubiquitin receptor for substrate recruitment. Importantly, this mutant enzyme exhibits wild-type levels of basal ATP hydrolysis, which is stimulated by the presence of an ubiquitinated substrate (Supplementary Figure 2b). By solving a high-resolution cryo-EM structure, we confirmed that the structural organization of this mutant enzyme in the absence of substrate was indistinguishable from the wild-type holoenzyme, except for the lack of Rpn13 (Supplementary Figure 3a).

For the substrate-bound structure of the mutant proteasome, we reduced the background around imaged particles by using a simplified substrate (Supplementary Figure 3c), containing a 52 aminoacid flexible tail at the C-terminus, a small globular domain (N1 domain of the gene-3-protein, G3P), and a single lysine at the N-terminus that allowed for homogeneous ubiquitination. Wild-type proteasome efficiently degrades this substrate in C- to N-terminal direction at a rate of ~1 min^{-1} $enzyme^{-1}$ (Supplementary Figure 4a), whereas the $Rpn11^{AXA}$ Rpn13Δ mutant proceeds through the globular domain and stalls when the N-terminally attached ubiquitin chain reaches the entrance to the pore. We therefore do not expect to observe electron density for the globular domain of the substrate. However, the presence of stalled substrate on the mutant proteasome was confirmed by pull-down experiments (Supplementary Figure 4b).

Rearrangement of the regulatory particle

Our subnanometer-resolution cryo-EM reconstruction reveals that substrate induces broad changes in the structure of the regulatory particle (Figure 2a, Supplementary Figure 3b, 5a–c), leading to a coaxial alignment of the DUB Rpn11, the N-ring, the AAA+ ring, and the entrance to the peptidase (Supplementary Movie 1). The N-ring is shifted and tilted by 16 Å and 13 degrees, respectively, and this movement is further propagated to the upper part of the regulatory particle through the N-terminal coiled coil of Rpt3 and Rpt6 (Figure 2b). This coiled coil suspends Rpn2 above the unfoldase [20], and the change in position of the N-ring

causes it to twist and hence Rpn2 to rotate. Since Rpn2 forms static interactions with the lid subunits Rpn3, Rpn11, Rpn12, as well as the bundle of lid-subunit C-termini [25], the movement of Rpn2 translates into a 25 degree rotation of the lid around the Rpt3–Rpt6 coiled coil anchor point (Figure 2c). Excluded from this rotation are the N-terminal domains of Rpn5 and Rpn6, which contact the AAA+ ring and the core peptidase and therefore perform distinct motions to accommodate the reorganization of subcomplexes. While we examined the 20S peptidase in detail, we did not observe any interpretable changes in the density of this subcomplex (Supplementary Figure 3b).

To eliminate the possibility that this new conformation is an alternative apo state, we searched the data sets of substrate-free proteasome particles for this conformer. In fact, we did observe particles in this new conformation, but there is a strict correlation with the presence of additional density at the entrance of the pore, in a location similar to the previously observed density for the GFP model substrate (Supplementary Figure 5d). It is therefore likely that this additional density results from endogenous substrates that co-purify with proteasomes from yeast, and we were able to confirm the presence of these ubiquitinated proteins in our proteasome preparations by anti-ubiquitin western blotting (Supplementary Figure 5e). Together, these findings indicate that the new conformation is not simply an alternative apo state, but a previously undescribed degradation mode that is induced by substrate.

We do not observe density for the unstructured polypeptide in the central pore, which is not surprising given the probable heterogeneity in its orientation in the pore and the limited resolution of the EM reconstruction. However, we used crosslinking and partial-degradation experiments to confirm that the substrate polypeptide is indeed translocated through the central pore (Supplementary Figure 6a,b). We therefore propose that the observed conformational switch originates from interactions between substrate and the AAA+ domains of Rpt1–6. Unfoldases of the AAA+ family are known to respond to substrate engagement with an increase in ATPase activity [35–37], potentially due to better subunit coordination in an altered ring conformation (see section on base reorganization below). ATP hydrolysis could thus be used to drive the conformational switch of the regulatory particle into a degradation-competent state after substrate contacts ATPase subunits in the central pore. Ubiquitin binding to the only receptor on our mutant proteasome, Rpn10, is unlikely to induce the conformational switch, because its ubiquitin-interacting motif (UIM) is flexibly attached and, in contrast to its globular domain, unresolved even in the substrate-bound state. If ubiquitin binding triggered the switch to the observed conformation, it would in fact hinder substrate engagement, because access to the N-ring pore becomes considerably restricted by Rpn11 (Figure 1). Furthermore, there are several examples for efficient ubiquitin-independent protein degradation by the proteasome [38–41]. Thus, for the ubiquitin-dependent majority of proteasome substrates, ubiquitin binding seems to be required for efficient engagement primarily because it increases the local substrate concentration at the proteasome surface and maximizes the probability that a flexible segment enters the processing pore.

Repositioning of Rpn11

In the substrate-free conformation of the regulatory particle, Rpn11 is located to the side of the N-ring pore. Docking the crystal structure of a related DUB, AMSH-LP [42], into this structure revealed that the Rpn11 catalytic groove is positioned directly above the bottom portion of the N-terminal coiled coil of Rpt4 and Rpt5 [20] (Figure 3a), which may prevent a substrate-bound ubiquitin from reaching the DUB active site. Importantly, however, in this pre-engaged state the N-ring pore is accessible to the flexible tail of an incoming substrate that is tethered to an ubiquitin receptor.

Upon substrate engagement by the AAA+ ring, Rpn11 shifts by 18 Å towards the center of the regulatory particle, placing it directly above the N-ring pore and liberating its active site for ubiquitin cleavage (Figure 3a, Supplementary Movie 1). This dramatic movement of Rpn11 may explain the previously described translocation dependence of deubiquitination [24] and offers a mechanism to prevent the premature removal of ubiquitin from a substrate that is not yet engaged.

In the substrate-engaged conformation, the catalytic groove of Rpn11 is aligned with the axis of the unfoldase pore, and an ubiquitin moiety bound with its C-terminal tail in this groove would be positioned alongside Rpn11, where it would have no steric clashes or interactions with other subunits of the regulatory particle (Figure 3b). This lack of interactions may explain the absence of observable electron density for the Rpn11-bound ubiquitin moiety, as its globular domain can adopt a wide range of orientations. However, we do observe a continuum of EM density across the catalytic groove (Figure 3c, Supplementary Figure 7a). Based on the crystal structure of ubiquitin-bound AMSH-LP [42], and given the fact that the tertiary organization of Rpn11 does not change upon substrate engagement (Supplementary Figure 7b,c), the additional bridging density may correspond to a short three-stranded beta sheet formed between Rpn11 and the C-terminal tail of ubiquitin. Besides this defined interaction with Rpn11, the ubiquitin chain appears to make no additional rigid contacts with other proteasome subunits. Even the receptor UIM of Rpn10 is unresolved in EM reconstructions due to its flexible attachment, which explains the lack density for an ubiquitin chain bound to it.

The placement of Rpn11 above the N-ring positions its active site only ~10 Å from the pore entrance, such that the isopeptide branch point of a substrate-attached ubiquitin must pass by the catalytic groove en-route to the central pore. Rpn11 may thus act as a gatekeeper, scanning the substrate polypeptide to ensure that all ubiquitins are removed before reaching and obstructing the entrance to the pore. In addition, the location of the Rpn11 active site likely determines its specificity for cleaving the proximal ubiquitin [26], since endo-isopeptidase activity would require the positioning of a second ubiquitin below Rpn11, in a region that is sterically occluded by the N-ring (Figure 3b).

Translocation-competent state of the base

Our EM structure reveals that substrate engagement in the central pore triggers major changes in the conformation of the AAA+ ring, primarily by inducing the subunits to shift and rotate away from the lid (Supplementary Movie 1). This movement of subunits leads to

a global shift of the AAA+ ring relative to the peptidase, from a 10-Å offset to a nearly perfect coaxial alignment (Figure 4a,b). Despite this transition, the C-terminal tails of Rpt2, Rpt3, and Rpt5, which contain the conserved HbYX (hydrophobic-tyrosine-unspecified residue) motif for peptidase interaction, remain docked in their respective binding pockets (Supplementary Figure 8a). Importantly, the Rpt motions result in a ~ 4-fold widening of the central pore, from an almost closed to an open state that can readily accommodate a translocating polypeptide (Figure 4b). Notably, the pore diameter in both the pre-engaged and substrate-bound conformation is actually smaller than it appears in our structures, since heterogeneity in the position of pore loops causes some lack of density in the central channel. In addition to the motions of the AAA+-domain hexamer, the rigid N-ring also shifts to become aligned with the peptidase, creating a continuous channel through the entire complex (Figure 4a). Together, this coaxial alignment and the expansion of the central pore most likely facilitate efficient substrate translocation (Supplementary Figure 8b).

The lid subcomplex appears to play an important role in stabilizing the reorganized architecture of the base. We observe three major interactions between the lid and the base in both the substrate-free and substrate-bound reconstructions. The small AAA+ subdomain of Rpt3 contacts the lid subunits Rpn5 and Rpn6, while the Rpt3–Rpt6 AAA+ interface interacts with Rpn7 (Figure 5). During the substrate-induced conformational transition, Rpn7 remains in contact with the Rpt3–Rpt6 interface and thus may function as a joint to accommodate the differential movements of the lid and base subcomplexes. In contrast, the base movements cause Rpt3 to switch its contacts with Rpn5 and Rpn6 to new binding sites that are located 30 and 25 Å further toward the respective PCI domains. Thus we define two distinct modes of interaction between the lid and the base, stabilizing the ATPase ring in either its pre-engaged state or in a translocation-competent conformation that is maintained throughout substrate processing.

An important consequence of the substrate-induced rotation of Rpt subunits is that the interfaces between the AAA+ domains become highly uniform around the ring (Figure 6a). These uniform interfaces are reminiscent of the “rigid bodies” that are formed in the homohexameric unfoldase ClpX between each large AAA+ subdomain and the small subdomain of the neighboring subunit [43]. Based on rigidifying intersubunit crosslinking of the ClpX hexamer, it has been proposed that ATP hydrolysis changes the relative orientation of the large and small AAA+ subdomains within a given subunit and thus drives movements of the “rigid body” formed with the subdomain of the neighbor to propel a substrate polypeptide through the central pore [43,44]. The apparent formation of uniform intersubunit contacts in the proteasomal Rpt ring upon substrate engagement therefore strongly suggests the transition from a pre-engaged to a more symmetrical, translocation-competent state that allows optimal coordination between ATPase subunits. Interestingly, one of the interfaces, between the small AAA+ subdomain of Rpt3 and the large AAA+ subdomain of Rpt4 (Figure 6b), already exhibits this “rigid body” orientation in the substrate-free state of the AAA+ ring. Rpt3 and Rpt4 are located at the top of the spiral staircase adopted by the Rpts prior to substrate engagement and would therefore be the first subunits to interact with an incoming substrate [20]. Substrate-induced movement of their stably associated large and small AAA+ subdomain may propagate the formation of uniform interfaces to the remainder

of the Rpts and thus induce the transition to a translocation-competent ring conformation that is then maintained until the substrate has been completely translocated.

Importantly, as the Rpt-ring conformation changes in response to substrate engagement, each AAA+ subunit rotates to a variable degree. This results in a switch from the pronounced spiral staircase of subunits in the substrate-free state to a nearly planar ring when substrate is engaged (Figure 7, Supplementary Movie 1). The strong pitch of the spiral in the absence of substrate originates from the large AAA+ subdomains of Rpt1–Rpt6 being arranged at different heights along the central pore axis, with Rpt3 at the top and Rpt2 at the bottom position [20,25]. In contrast, the large AAA+ subdomains in the substrate-engaged conformation are at one level, but each tilted to different degrees about an axis lying in the plane of the ring (Figure 7). This variable tilting results in a new spiral arrangement of the pore loops, with Rpt1 now assuming the uppermost position and Rpt4 at the bottom. Despite their structural differences, both ring conformations contain a bridging subunit that connects the top and bottom of the spiral. Rpt6 and Rpt5 fill this intermediate position in the substrate-free and substrate-bound states, respectively.

Spiral staircase arrangements have been observed in the crystal structures of the DNA-bound RecA-type helicases Rho and DnaB, as well as the AAA+ helicase E1, with translocation proposed to involve large-scale motions as subunits successively pass through the different conformational registers of the spiral [27–29]. Surprisingly, the ATPase ring of the 26S proteasome in the substrate-engaged state displays a fixed spiral orientation with highly ordered densities (Figure 7b). This is especially interesting given that substrate stimulates the ATPase rate (Supplementary Figure 2b), and the enzyme was hydrolyzing at this stimulated rate when the sample was frozen for EM analysis. The vitrification within ~0.2 ms is fast enough to prevent thermally-induced rearrangements and thus provides a true snapshot of the translocating proteasome. While it is possible that substrate translocation is driven by only local motions of the pore-loops in an otherwise fixed AAA+ spiral, it is more likely that the spiral is dynamic and the specific orientation we observe in our structure represents a “dwell” state, adopted before or after coordinated ATP hydrolysis events that rapidly progress around the ring. The uniform subunit interfaces formed between neighboring Rpts upon substrate engagement are consistent with this model, as they would facilitate such coordinated firing of subunits. A rapid progression of ATP-hydrolysis-driven conformational changes around the ring has been proposed for the AAA+ DNA packaging motor of the bacteriophage φ29 [45,46]. During translocation of a DNA substrate, this packaging motor spends 90% of its time in a stationary or “dwell” phase, during which ADP is released and subunits are loaded with ATP, and only 10% of its time in a “burst” phase, during which substrate is translocated by coordinated conformational changes of subunits around the ring. A similar temporal distribution for the substrate-engaged proteasome, with 90% of particles in the dwell phase at any given time, would result in an EM reconstruction with an apparently fixed AAA+-ring spiral, as we observe. However, particles that are in the burst phase at the time of sample freezing may cause the lower local resolution we observe for the AAA+ ring in the substrate-bound compared to the pre-engaged structure (Supplementary Figure 5a,b). The pre-engaged state may not exhibit a coordinated burst phase or undergo the same conformational changes associated with a rapid, progressive

hydrolysis around the ring, because its individual subunits are not coupled by the uniform interfaces that are present in the substrate-engaged state.

The specific orientation of the translocation-competent spiral, with Rpt1 adopting the top position in all dwell-phase particles, likely originates from conformational constraints imposed by the heterohexameric architecture of the ATPase ring as well as its asymmetric surroundings. We propose that the Rpt ring adopts this spiral as soon as a substrate polypeptide is engaged in the central pore. Coordinated ATP hydrolysis then drives the tilting of individual AAA+ domains through the different subunit registers of the translocation-competent spiral, generating a power stroke that propels a certain length of polypeptide through the pore. After each stroke, the ring returns to the dwell-phase conformation with Rpt1 in the top position. Repeating this process thus drives the stepwise translocation of substrate into the peptidase. After the substrate has been completely translocated, the AAA+ ring, together with the rest of the regulatory particle, switches back to the pre-engaged conformation with a pronounced spiral staircase ready to accept the next incoming substrate.

Discussion

The work presented here provides the first insights into the structure of the actively translocating 26S proteasome and outlines the transitions that accompany substrate engagement (Figure 8, Supplementary Movie 1). Importantly, these new data help us to identify all previously described structures as representatives of a pre-engaged state with features that facilitate substrate engagement but are incompatible with further processing [20–22,25,47]. In this pre-engaged state, the entrance to the N-ring is accessible to the unstructured initiation region of an incoming substrate whose ubiquitin chain is tethered to a proteasomal receptor. However, the central pore of the ATPase ring is constricted and not coaxially aligned with the subjacent peptidase. Furthermore, the DUB Rpn11 active site is occluded, preventing premature deubiquitination of the substrate prior to engagement by the ATPase ring. In this state, the AAA+ domains are arranged in a pronounced spiral staircase. Substrate interactions with Rpt subunits at the top of this spiral trigger the switching of the regulatory particle into a translocation-competent conformation that is characterized by a reorganized AAA+ ring with an alternative spiral arrangement, more uniform AAA-domain interfaces, and a continuous central channel to the peptidase (Figure 8). Rpn11 shifts to a central location directly above the N-ring pore, where its active site is accessible and ideally positioned to scan translocating polypeptides for ubiquitin chains, ensuring complete deubiquitination. This substrate-engaged conformation of the regulatory particle is stabilized by an alternative set of lid-base interactions.

A similar proteasome conformation with a rearranged AAA+ ring and a continuous central channel has recently been observed in the presence of the slowly-hydrolysable ATPγS [48], which we assume traps the ATPase motor in a dwell-phase-like state. Based on these data and our substrate-bound structure of the 26S proteasome, we conclude that a spiral arrangement of ATPase subunits is functionally relevant for translocation. Our data are consistent with a mechanism in which a fast, highly coordinated wave of ATP-hydrolysis-induced conformational changes around the ATPase ring propels the substrate through the

central pore and into the peptidase. We propose that related AAA+ protein unfoldases operate by similar mechanisms, and in fact, recent single-molecule data for the unfoldase ClpX agree with this model of translocation (R. Maillard, K. Nyquist, M. Sen, C. Bustamante, and A. Martin, University of California, Berkeley, California, USA, unpublished results). While future biophysical and biochemical studies will be necessary to describe the detailed mechanisms involved in proteasomal engagement and translocation of substrate, the data presented here offer an important structural framework for understanding these events.

Online Methods

Yeast strain construction

Genotypic information for every strain used in this study is provided in Supplementary Table 1. Wild-type proteasome holoenzyme was purified from the strain YYS40 *(MATa ade2-1 his3-11,15 leu2-3,112 trp1-1 ura3-1 can1-100 RPN11:RPN11-3XFLAG (HIS3)*) [50]. To generate the strain used to purify Rpn11AXA Rpn13Δ holoenzyme, the *RPN11* promoter, coding sequence, and terminator were cloned into pRS304 (*TRP1*). A 3XFLAG tag was inserted at the *RPN11* C-terminus, and the two conserved active-site histidines (defined by EX*n*HXHX10D) were mutated to alanine (H109A, H111A). This plasmid was then integrated at the *TRP1* locus in the strain DOM90, resulting in a strain that contained both wild-type *RPN11* and a tagged *RPN11-AXA* mutant under control of its endogenous promoter. Rpn13 was deleted from this strain by integrating the *KanMX6* sequence at the *RPN13* genomic locus, resulting in the strain yAM11 (*MAT***a** *ade2-1 his3-11,15 leu2-3,112 ura3-1 can1-100 trp1-1::PRPN11-rpn11AXA-3XFLAG-TRP1(pRS304) rpn13*Δ*::KanMX)*.

Proteasome purification

Wild-type and mutant proteasome was purified from *S. cerevisiae* essentially as described [20]. For holoenzyme purification, yeast cells from strains containing a 3XFlag-tag on Rpn11 were lysed using a SPEX Freezer/Mill (catalog #6870). Lysed cells were resuspended in lysis buffer containing 60 mM HEPES pH7.6, 50 mM NaCl, 50 mM KCl, 5 mM MgCl2, 0.5 mM EDTA, 10% glycerol, 0.2% NP-40, and an ATP regeneration mix (5 mM ATP, 0.03 mg/ml creatine kinase, 16 mM creatine phosphate). Holoenzyme was bound to anti-Flag M2 affinity resin (Sigma) and washed with wash buffer (60 mM HEPES pH 7.6, 50 mM NaCl, 50 mM KCl, 5 mM MgCl2, 0.5 mM EDTA, 10% glycerol, 0.1% NP-40 and 500 mM ATP) before elution with Flag peptide and separation by size-exclusion chromatography over Superose-6 in gel-filtration (GF) buffer (60 mM HEPES pH 7.6, 50 mM NaCl, 50 mM KCl, 5 mM MgCl2, 0.5 mM EDTA, and 500 mM ATP) containing 5% glycerol.

Purification, ubiquitination, and degradation of model substrates

The GFP–titin–cyclin fusion substrate was purified by Ni-NTA affinity chromatography, followed by size-exclusion chromatography as described [20]. The substrate (45 μM) was modified with polyubiquitin chains using 45 μM yeast Rsp5, 1 μM yeast Uba1, 30 μM yeast Ubc4, and 250 μM ubiquitin (a 10:1 mixture of wild-type to methyl- ubiquitin, in order to reduce the formation of very long ubiquitin chains). Degradation of the ubiquitinated GFP-

fusion substrate by wild-type proteasome in GF buffer at 30° C and in the presence of an ATP-regeneration system (5 mM ATP, 16 mM creatine phosphate, 6 mg/ml creatine phosphokinase) was monitored by the loss of fluorescence, using a QuantaMaster spectrofluorimeter (PTI). The alternative substrate, consisting of the N1-domain of G3P fused to cyclin, was purified by Ni-NTA affinity, followed by size exclusion chromatography. This substrate (75 μM) was ubiquitinated on its single lysine using 175 nM yeast Rsp5, 170 nM yeast Uba1, 5 μM yeast Ubc4, and 1.2 mM ubiquitin (a 10:1 mixture of wild-type to methyl- ubiquitin). Degradation was monitored by SDS-PAGE and coomassie staining. This substrate was also labeled on an N-terminal cysteine with Cy5-maleimide (GE Healthcare, product code PA25031) for fluorescence visualization. Substrate was buffer exchanged to remove reducing agent and incubated with Cy5-maleimide for 1 hour at room temperature in the dark. The sample was then reduced with 10 mM DTT to neutralize excess dye and buffer-exchanged using a PD-10 column to remove free dye for subsequent ubiquitination. This substrate was imaged on a Typhoon Trio Variable Mode Imager (GE healthcare) using a 670 nm band pass filter.

ATP hydrolysis assay

ATPase activity was quantified using an NADH-coupled ATPase assay. 300 nM proteasome holoenzyme was incubated with 1x ATPase mix (3 U ml^{-1} pyruvate kinase, 3 U ml^{-1} lactate dehydrogenase, 1 mM NADH, 7.5 mM phosphoenol pyruvate) at 30°C, in the presence or absence of 10 μM ubiquitinated substrate. Absorbance at 340 nm was monitored for 900 sec at 5 sec intervals using a UV-Vis Spectrophotometer (Agilent).

Crosslinking

G3P substrate was either ubiquitinated or mock-ubiquitinated by adding all ubiquitination components except ubiquitin. Substrate was then dialyzed for 30 min into GF buffer to remove DTT, and the cysteine residue was activated for cross-linking by incubation with 1mM 5,5′-dithiobis-(2-nitrobenzoic acid) (DTNB) for 5 min at room temperature. Substrate was then dialyzed again into GF buffer to remove free DTNB. Proteasomes containing $Rpn11^{AXA}$ and HA-tagged Rpt1 with either a wild-type or cysteine-mutant pore loop (Rpt1 Y283C) (purified from yAM12 and yAM13, respectively) were buffer exchanged to remove reducing agent. DTNB-activated substrate (~10 μM) was then mixed with proteasome (~1 μM) in the presence of an ATP-regeneration system, and substrate translocation and cross-linking was allowed to proceed for 30 min at 30 °C, before the reaction was stopped by the addition of 200 mM iodoacetic acid. Samples were boiled after the addition of 2X sample buffer and 5 M urea for separation by non-reducing SDS-PAGE. Rpt1 subunits with cross-linked substrate were detected by western blotting with an anti-HA antibody (12CA5, Santa Cruz Biotechnology, catalog # sc-57592) at 1:10,000.

Sample preparation for cryo-EM analysis

Frozen-hydrated preservation of wild type and $Rpn11^{AXA}$ Rpn13Δ proteasome particles in the absence and presence of substrate was performed in a similar manner. In the case of wild type, 6 μl of 8 μM purified holoenzyme in GF buffer (60 mM HEPES, pH 7.6, 50 mM NaCl, 50 mM KCl, 5 mM $MgCl_2$, 0.5 mM EDTA, 1 mM DTT, 0.5 mM ATP) with 2.5% glycerol was incubated with 15 μl of 6 μM ubiquitinated GFP–cyclin substrate that had been dialyzed

against QAH buffer (20mM HEPES, pH 7.6, 150 mM NaCl, and 1mM MgCl). The holoenzyme and substrate were incubated at room temperature for 5 minutes, at which point excess un-engaged substrate was depleted by the addition of 1 μl of 2X magnetic bead slurry (MagneHis™ Ni-Particles, Promega) and immediately plunge-frozen. The C-terminal His-tag located at the end of the substrate's unstructured engagement regions would be blocked from interacting with the beads upon engagement by the proteasome, allowing depletion of only un-engaged substrate. Purified Rpn11^{AXA} Rpn13Δ holoenzyme was diluted from a concentration of 18 μM in GF with 5% glycerol to a concentration of 1.8 μl in EM buffer (GF with 0.05% NP40, 2mM ATP, and 0% glycerol). 38.8 μl of diluted holoenzyme was incubated with 1.3 μl of 46 μM G3P substrate in EM buffer for 5 minutes and immediately plunge-frozen.

All samples were plunge-frozen on 400-mesh C-flats (Protochips Inc.) containing 2um holes with a spacing of 2um and had been plasma cleaned in a 75% argon/25% oxygen atmosphere at 15 Watts for 6 seconds using a Solarus plasma cleaner (Gatan, Inc). 3μl aliquots of the samples were applied to these hydrophilized grids, blotted for 3 seconds with Whatman No.1 filter paper, and plunged into liquid ethane using a Vitrobot (FEI co). The Vitrobot environment chamber was programmed to maintain a temperature of 4°C and 100% humidity, and use a blotting offset of –1. Grids were stored in liquid nitrogen until being loaded into a Gatan 626 single tilt cryotransfer holder for data collection.

Cryo-electron microscopy data collection and processing

Frozen grids were inserted into a Tecnai F20 Twin transmission electron microscope operating at 120keV, and data were collected on a Gatan 4kx4k CCD using the MSI-T application within the Leginon automated electron microscopy package [51]. Wild type proteasome particles in the presence of substrate were acquired at a nominal magnification of 80,000X (1.45 Å per pixel at the specimen level), and all Rpn11^{AXA} Rpn13Δ were collected at 100,000X (1.08 Å per pixel). All imaging used an electron dose of 20 $e^{-}/Å^{2}$ with a randomly set focus ranging from −1.2 to −2.5 μm. A total of 3439, 4740, and 5328 micrographs were collected for the wild type + substrate, Rpn11^{AXA} Rpn13Δ, and Rpn11^{AXA} Rpn13Δ + substrate samples, respectively, using the MSI-T application of the Leginon software [51].

All pre-processing of data leading up to the three-dimensional reconstruction was performed within the Appion processing environment [52]. The contrast transfer function (CTF) of each micrograph was estimated with ACE2 concurrently with data collection. Forward-projections of a previously solved proteasome structure [20] were used to generate templates for cross-correlation-based automated particle selection [53]. Carbon edges were masked out from the micrographs manually, and particles appearing within these regions were not considered for analysis. Micrographs that showed an 80% confidence in CTF estimation accuracy were extracted using a box size of 576 pixels for the wild type data, and 640 pixels for the Rpn11^{AXA} Rpn13Δ data. The resulting stacks of 98632, 112015, and 282600 particles (for the wild type + substrate, Rpn11^{AXA} Rpn13Δ, and Rpn11^{AXA} Rpn13Δ + substrate, respectively) were each binned by a factor of two, and the particles were

normalized to remove pixels whose values were above or below 4.5 sigma of the mean pixel value using the XMIPP normalization program [54].

Each dataset was processed independently, beginning with removal of false positives from automated particle selection, aggregates, and singly capped particles. This was accomplished through two-dimensional classification using several rounds of iterative multivariate statistical and analysis (MSA) and multi-reference alignment (MRA) using the IMAGIC software package [55]. Class averages depicting detailed views of doubly-capped proteasomes were manually selected, and particles contributing to these views were used to generate a new stack. This new stack was subjected to MSA-MRA analysis, and again particles contributing to detailed class averages were separated into a new stack. Several rounds of classification in this manner resulted in a final stacks of 63918, 80011, and 188400 particles for the wild type + substrate, Rpn11^{AXA} Rpn13Δ, and Rpn11^{AXA} Rpn13Δ + substrate, respectively. To inspect the conformational heterogeneity of the regulatory particles within these datasets, well-resolved class averages containing 200–400 particles depicting side-views of the proteasome were selected and the aligned particles contributing to each average were saved as an individual stack. Inspection of class averages calculated from the aligned particles for each stack showed that the regulatory particle of wild-type particles in the presence of substrate showed considerably more variability than the Rpn11^{AXA} Rpn13Δ particles (Supplementary Figure 1a–c).

Three-dimensional processing of the wild type + substrate dataset

The conformational differences observed within the regulatory particle of the wild type proteasome particles in the presence of substrate were not clear enough to correlate distinct structural changes between the many holoenzyme orientations presented in the class averages, so projection-matching of the 1000 class averages was used to arrive at an asymmetric model of the wild type substrate-engaged proteasome. The previous wild type reconstruction (EMDB-1992) was low-pass filtered to 50Å resolution and used as a starting model for 5 rounds of projection matching using EMAN2 and SPARX libraries, with forward-projections generated at 15° increments. The resulting structure contained one regulatory particle reminiscent of the previously observed unbound state, while the other regulatory particle exhibited an altered organization (Supplementary Figure 1d). This low-resolution model was then used as a starting point for projection matching of the full dataset of 63918 particles, yielding an asymmetric 25Å resolution structure of the proteasome. This reconstruction showed with more detail the conformational differences between the regulatory particle, confirming that one remained in the previously observed unbound state, while the other assumed an alternate conformation, presumably due to interaction with substrate.

We next explored the possibility that this wild type dataset contained a mixture of substrate occupancy, in which some proteasome complexes were completely free of substrate and others contained substrate interactions at both regulatory particles. The asymmetric reconstruction was split into two densities through the center of the peptidase, and C2 symmetry was applied to each half-holoenzyme (Supplementary Figure 1d). The resulting substrate-free and doubly-bound proteasome densities, along with the half-bound

reconstruction, served as three seeds for multi-model projection matching using the full dataset of wild type particles with EMAN2 and SPARX libraries. No symmetry was enforced during this process in order to allow regression of the C2-symmetric initial models to a half-bound state in the case that such occupancies did not exist. At the conclusion of the refinement the conformational organizations observed in the final densities reflected those of the three initial models, with 25589 (40%), 22367 (35%), and 15962 (25%) of the particles as half-bound, substrate-free, and doubly-bound, respectively. Due to a preservation of C2 symmetry in the substrate-free and doubly-bound reconstructions, this symmetry was imposed during a final refinement of the particle alignments in FREALIGN [56].

Three-dimensional processing of the Rpn11^{AXA} Rpn13Δ datasets

Three-dimensional reconstructions of the substrate-free and substrate-engaged Rpn11^{AXA} Rpn13Δ particle datasets were performed using EMAN2 and SPARX libraries, as described previously [20]. To minimize the introduction of model bias during the projection matching, the previously determined wild type reconstruction (EMDB-1992) was low-pass filtered to 50Å resolution for use as a starting point for refinement of both datasets. A final refinement of the substrate-free and substrate engaged particle alignments was performed in FREALIGN. C2 symmetry was enforced during all refinements, and the resolutions of the final reconstructions were estimated to be about 9Å, based on “gold-standard” Fourier shell correlation calculations (cutoff at 0.143) from two independent refinements of half-datasets [57]. A local resolution assessment of the reconstructions indicated that different components of the structures ranged in resolution from 7 to 12 Å, and were low-pass filtered accordingly (Supplementary Figure 5a-b). Local resolution calculations and localized low-pass filtering for all reconstructions were performed using the “blocres” and “blocfilt” functions of the Bsoft package [58]. Notably, the addition of substrate appears to narrow the angular distribution of proteasome particles in vitreous ice, as shown in Supplementary Figure 5c, providing a possible explanation for the unimproved resolution of the substrate-engaged dataset relative to the substrate-free dataset, despite containing substantially more particles.

In order to investigate the possibility that the conformation we observe for the substrate-engaged particles is in fact an alternative apo-state conformation, we reprocessed substrate-free wild type and AXA mutant particle datasets using multi-model projection matching. The three models used for this refinement included a C2-symmetric proteasome containing two apo-state regulatory particles (EMDB-1992), a C2-symmetric proteasome containing two substrate-engaged regulatory particles (the substrate-engaged Rpn11^{AXA} Rpn13Δ reconstruction), and an asymmetric proteasome containing one apo-state and one substrate-engaged regulatory particle. The three structures were low-pass filtered to 15Å so that the distinctive structural aspects that define each state could drive the separation of particles. These models contained a built-in control that would signify the presence of model bias during the reconstruction, since the apo-state regulatory particle density contained Rpn13 while the substrate-engaged state did not. At the end of the refinement, all wild-type reconstructions should contain Rpn13, regardless of state, and this subunit should be absent from all the mutant reconstructions. The same EMAN2/SPARX projection-matching algorithm that was used for the C2-symmetric reconstructions was used, although no

symmetry was enforced, and particles were sorted into one of three input models. The three asymmetric back-projections were then used for the next round of projection matching and sorting.

Unexpectedly, a notable percentage of the proteasome particles from both datasets were classified to the model containing one apo-state and one substrate-engaged regulatory particle (the apo/substrate state). 29% and 46% of the substrate-free wild type & mutant datasets contained proteasomes in this apo/substrate state, respectively. For each of these reconstructions, a globular density near the entrance to the ATPase pore accompanies the substrate-engaged regulatory particle, similar to the density attributed to GFP in the previously described wild type reconstruction in the presence of substrate (see Supplementary Figure 5d). It is not possible that this density is a product of model bias, as the substrate-engaged mutant density used to generate the initial models did not contain this globular density due to the design of the substrate. The strict correlation between the appearance of this globular density and the rearranged proteasome conformation suggests that these regulatory particles were bound to endogenous substrate during the purification and freezing for imaging. Notably, there were insufficient fully substrate-engaged proteasomes (bound to both regulatory particles) in either dataset to form a stable three-dimensional model during the refinement. From the initial set of “apo” wild type particles, 69485 and 28321 particles contributed to the final backprojection of the apo and apo/substrate reconstructions, respectively. From the initial set of “apo” mutant AXA particles, 33435 and 28312 particles contributed to the final backprojection of the apo and apo/substrate reconstructions, respectively. The substrate-free subset of particles was extracted and reprocessed imposing C2 symmetry to boost the signal to noise ratio and improve the overall resolution of the reconstruction.

The same methodology was used to determine the percentage of apo-state regulatory particles in the AXA mutant + substrate dataset, but none were found. 132310 particles contributed to the final back projection of the substrate-bound AXA mutant reconstruction. For all reconstructions described, low-resolution Fourier amplitudes of the final densities were dampened to match those of a generic protein using the SPIDER software package [59]. Based on a previous segmentation of the subunits [20], segmentation of the densities was performed manually using the volume tracer tool of the UCSF Chimera visualization software [60].

Supplementary Material

Refer to Web version on PubMed Central for supplementary material.

Acknowledgments

We thank C. Bashore (University of California Berkeley, California, USA) for providing the construct for the G3P model substrate. We thank E. Nogales for thoughtful discussions and providing access to her EM facility. Finally, we thank the members of the Martin lab for helpful comments. M.E.M. acknowledges support from the American Cancer Society (grant 121453-PF-11-178-01-TBE), and G.C.L. is supported as a Damon Runyon Cancer Research Foundation Fellow (DRG 2055-10). This research was funded in part by the Searle Scholars Program (A.M.), start-up funds from the University of California Berkeley Molecular and Cell Biology Department (A.M.), the US National Institutes of Health grant R01-GM094497-01A1 (A.M.), the NSF CAREER Program NSF-MCB-1150288 (A.M.), and the Lawrence Berkeley National Laboratory (G.C.L.).

References

1. Finley D. Recognition and processing of ubiquitin-protein conjugates by the proteasome. Annu Rev Biochem. 2009; 78:477–513. [PubMed: 19489727]
2. Sauer RT, Baker TA. AAA+ proteases: ATP-fueled machines of protein destruction. Annu Rev Biochem. 2011; 80:587–612. [PubMed: 21469952]
3. Saeki Y, Tanaka K. Assembly and function of the proteasome. Methods Mol Biol. 2012; 832:315–37. [PubMed: 22350895]
4. Groll M, et al. A gated channel into the proteasome core particle. Nat Struct Biol. 2000; 7:1062–7. [PubMed: 11062564]
5. Thrower JS, Hoffman L, Rechsteiner M, Pickart CM. Recognition of the polyubiquitin proteolytic signal. Embo J. 2000; 19:94–102. [PubMed: 10619848]
6. Smith DM, Benaroudj N, Goldberg A. Proteasomes and their associated ATPases: a destructive combination. J Struct Biol. 2006; 156:72–83. [PubMed: 16919475]
7. Glickman MH, et al. A subcomplex of the proteasome regulatory particle required for ubiquitin-conjugate degradation and related to the COP9-signalosome and eIF3. Cell. 1998; 94:615–23. [PubMed: 9741626]
8. Glickman MH, Rubin DM, Fried VA, Finley D. The regulatory particle of the Saccharomyces cerevisiae proteasome. Mol Cell Biol. 1998; 18:3149–62. [PubMed: 9584156]
9. Tomko RJ Jr, Funakoshi M, Schneider K, Wang J, Hochstrasser M. Heterohexameric ring arrangement of the eukaryotic proteasomal ATPases: implications for proteasome structure assembly. Mol Cell. 2010; 38:393–403. [PubMed: 20471945]
10. Hamazaki J, et al. A novel proteasome interacting protein recruits the deubiquitinating enzyme UCH37 to 26S proteasomes. Embo J. 2006; 25:4524–36. [PubMed: 16990800]
11. Leggett DS, et al. Multiple associated proteins regulate proteasome structure and function. Mol Cell. 2002; 10:495–507. [PubMed: 12408819]
12. Martin A, Baker TA, Sauer RT. Pore loops of the AAA+ ClpX machine grip substrates to drive translocation and unfolding. Nat Struct Mol Biol. 2008; 15:1147–51. [PubMed: 18931677]
13. Maillard RA, et al. ClpX(P) generates mechanical force to unfold and translocate its protein substrates. Cell. 2011; 145:459–69. [PubMed: 21529717]
14. Aubin-Tam ME, Olivares AO, Sauer RT, Baker TA, Lang MJ. Single-molecule protein unfolding and translocation by an ATP-fueled proteolytic machine. Cell. 2011; 145:257–67. [PubMed: 21496645]
15. Zhang F, et al. Mechanism of substrate unfolding and translocation by the regulatory particle of the proteasome from Methanocaldococcus jannaschii. Mol Cell. 2009; 34:485–96. [PubMed: 19481528]
16. Erales J, Hoyt MA, Troll F, Coffino P. Functional asymmetries of proteasome translocase pore. J Biol Chem. 2012; 287:18535–43. [PubMed: 22493437]
17. Zhang F, et al. Structural insights into the regulatory particle of the proteasome from Methanocaldococcus jannaschii. Mol Cell. 2009; 34:473–84. [PubMed: 19481527]
18. Smith DM, et al. Docking of the proteasomal ATPases' carboxyl termini in the 20S proteasome's alpha ring opens the gate for substrate entry. Mol Cell. 2007; 27:731–44. [PubMed: 17803938]
19. Rabl J, et al. Mechanism of gate opening in the 20S proteasome by the proteasomal ATPases. Mol Cell. 2008; 30:360–8. [PubMed: 18471981]
20. Lander GC, et al. Complete subunit architecture of the proteasome regulatory particle. Nature. 2012; 482:186–91. [PubMed: 22237024]
21. Bohn S, et al. Structure of the 26S proteasome from Schizosaccharomyces pombe at subnanometer resolution. Proc Natl Acad Sci U S A. 2010; 107:20992–7. [PubMed: 21098295]
22. Nickell S, et al. Insights into the molecular architecture of the 26S proteasome. Proc Natl Acad Sci U S A. 2009; 106:11943–7. [PubMed: 19581588]
23. Lasker K, et al. Molecular architecture of the 26S proteasome holocomplex determined by an integrative approach. Proc Natl Acad Sci U S A. 2012; 109:1380–7. [PubMed: 22307589]

24. Verma R, et al. Role of Rpn11 metalloprotease in deubiquitination and degradation by the 26S proteasome. Science. 2002; 298:611–5. [PubMed: 12183636]
25. Beck F, et al. Near-atomic resolution structural model of the yeast 26S proteasome. Proc Natl Acad Sci U S A. 2012; 109:14870–5. [PubMed: 22927375]
26. Yao T, Cohen RE. A cryptic protease couples deubiquitination and degradation by the proteasome. Nature. 2002; 419:403–7. [PubMed: 12353037]
27. Thomsen ND, Berger JM. Running in reverse: the structural basis for translocation polarity in hexameric helicases. Cell. 2009; 139:523–34. [PubMed: 19879839]
28. Enemark EJ, Joshua-Tor L. Mechanism of DNA translocation in a replicative hexameric helicase. Nature. 2006; 442:270–5. [PubMed: 16855583]
29. Itsathitphaisarn O, Wing RA, Eliason WK, Wang J, Steitz TA. The Hexameric Helicase DnaB Adopts a Nonplanar Conformation during Translocation. Cell. 2012; 151:267–77. [PubMed: 23022319]
30. Inobe T, Fishbain S, Prakash S, Matouschek A. Defining the geometry of the two-component proteasome degron. Nat Chem Biol. 2011; 7:161–7. [PubMed: 21278740]
31. Prakash S, Tian L, Ratliff KS, Lehotzky RE, Matouschek A. An unstructured initiation site is required for efficient proteasome-mediated degradation. Nat Struct Mol Biol. 2004; 11:830–7. [PubMed: 15311270]
32. Martin A, Baker TA, Sauer RT. Protein unfolding by a AAA+ protease is dependent on ATP-hydrolysis rates and substrate energy landscapes. Nat Struct Mol Biol. 2008; 15:139–45. [PubMed: 18223658]
33. Ortega J, Lee HS, Maurizi MR, Steven AC. Alternating translocation of protein substrates from both ends of ClpXP protease. EMBO J. 2002; 21:4938–49. [PubMed: 12234933]
34. Chandra A, Chen L, Liang H, Madura K. Proteasome assembly influences interaction with ubiquitinated proteins and shuttle factors. J Biol Chem. 285:8330–9. [PubMed: 20061387]
35. Kim YC, Li X, Thompson D, Demartino GN. ATP-binding by proteasomal ATPases regulates cellular assembly and substrate-induced functions of the 26S proteasome. J Biol Chem. 2012
36. Burton RE, Siddiqui SM, Kim YI, Baker TA, Sauer RT. Effects of protein stability and structure on substrate processing by the ClpXP unfolding and degradation machine. EMBO J. 2001; 20:3092–100. [PubMed: 11406586]
37. Hwang BJ, Woo KM, Goldberg AL, Chung CH. Protease Ti, a new ATP-dependent protease in Escherichia coli, contains protein-activated ATPase and proteolytic functions in distinct subunits. J Biol Chem. 1988; 263:8727–34. [PubMed: 2967816]
38. Janse DM, Crosas B, Finley D, Church GM. Localization to the proteasome is sufficient for degradation. J Biol Chem. 2004; 279:21415–20. [PubMed: 15039430]
39. Schneekloth JS Jr, et al. J Am Chem Soc. 2004; 126:3748–54. [PubMed: 15038727]
40. Zhang M, Pickart CM, Coffino P. Determinants of proteasome recognition of ornithine decarboxylase, a ubiquitin-independent substrate. Embo J. 2003; 22:1488–96. [PubMed: 12660156]
41. Henderson A, Erales J, Hoyt MA, Coffino P. Dependence of proteasome processing rate on substrate unfolding. J Biol Chem. 286:17495–502. [PubMed: 21454622]
42. Sato Y, et al. Structural basis for specific cleavage of Lys 63-linked polyubiquitin chains. Nature. 2008; 455:358–62. [PubMed: 18758443]
43. Glynn SE, Martin A, Nager AR, Baker TA, Sauer RT. Structures of asymmetric ClpX hexamers reveal nucleotide-dependent motions in a AAA+ protein-unfolding machine. Cell. 2009; 139:744–56. [PubMed: 19914167]
44. Glynn SE, Nager AR, Baker TA, Sauer RT. Dynamic and static components power unfolding in topologically closed rings of a AAA+ proteolytic machine. Nat Struct Mol Biol. 2012; 19:616–22. [PubMed: 22562135]
45. Moffitt JR, et al. Intersubunit coordination in a homomeric ring ATPase. Nature. 2009; 457:446–50. [PubMed: 19129763]
46. Chistol G, et al. High degree of coordination and division of labor among subunits in a homomeric ring ATPase. Cell. 2012; 151:1017–28. [PubMed: 23178121]

47. da Fonseca PC, He J, Morris EP. Molecular model of the human 26S proteasome. Mol Cell. 2012; 46:54–66. [PubMed: 22500737]
48. Sledz P, et al. Structure of the 26S proteasome with ATP-gammaS bound provides insights into the mechanism of nucleotide-dependent substrate translocation. Proc Natl Acad Sci U S A.
49. Pathare GR, et al. The proteasomal subunit Rpn6 is a molecular clamp holding the core and regulatory subcomplexes together. Proc Natl Acad Sci U S A. 2011; 109:149–54. [PubMed: 22187461]
50. Sone T, Saeki Y, Toh-e A, Yokosawa H. Sem1p is a novel subunit of the 26 S proteasome from Saccharomyces cerevisiae. J Biol Chem. 2004; 279:28807–16. [PubMed: 15117943]
51. Suloway C, et al. Automated molecular microscopy: the new Leginon system. J Struct Biol. 2005; 151:41–60. [PubMed: 15890530]
52. Lander GC, et al. Appion: an integrated, database-driven pipeline to facilitate EM image processing. J Struct Biol. 2009; 166:95–102. [PubMed: 19263523]
53. Roseman AM. FindEM--a fast, efficient program for automatic selection of particles from electron micrographs. J Struct Biol. 2004; 145:91–9. [PubMed: 15065677]
54. Sorzano CO, et al. XMIPP: a new generation of an open-source image processing package for electron microscopy. J Struct Biol. 2004; 148:194–204. [PubMed: 15477099]
55. van Heel M, Harauz G, Orlova EV, Schmidt R, Schatz M. A new generation of the IMAGIC image processing system. J Struct Biol. 1996; 116:17–24. [PubMed: 8742718]
56. Grigorieff N. FREALIGN: high-resolution refinement of single particle structures. J Struct Biol. 2007; 157:117–25. [PubMed: 16828314]
57. Scheres SH, Chen S. Prevention of overfitting in cryo-EM structure determination. Nat Methods. 2012; 9:853–4. [PubMed: 22842542]
58. Heymann JB, Belnap DM. Bsoft: image processing and molecular modeling for electron microscopy. J Struct Biol. 2007; 157:3–18. [PubMed: 17011211]
59. Frank J, et al. SPIDER and WEB: processing and visualization of images in 3D electron microscopy and related fields. J Struct Biol. 1996; 116:190–9. [PubMed: 8742743]
60. Goddard TD, Huang CC, Ferrin TE. Visualizing density maps with UCSF Chimera. J Struct Biol. 2007; 157:281–7. [PubMed: 16963278]

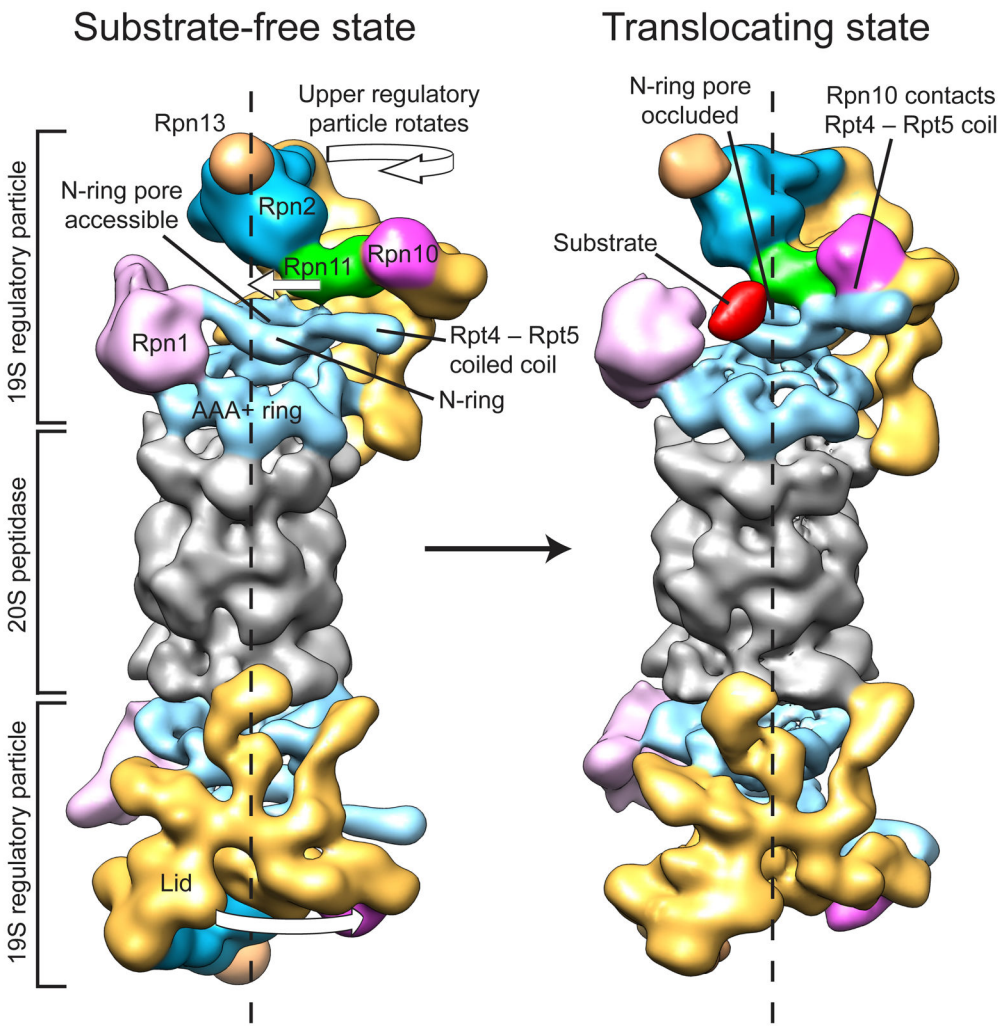

Figure 1. Conformational transition of the proteasome from a substrate-free to an actively degrading state

The structures of wild-type proteasome in its substrate-free (left) and substrate-engaged state (right) identically oriented based on their 20S peptidase (grey), with a dashed line indicating the central axis of the peptidase pore. Substrate engagement induces a conformational rearrangement of the regulatory particle, including a rotation of Rpn2 (dark blue), Rpn13 (light orange), and the lid subcomplex (yellow), the formation of contacts between the ubiquitin receptor Rpn10 (purple) and the Rpt4–Rpt5 coiled coil, and a coaxial alignment of the N-ring and the AAA+ ring (both cyan) with the peptidase. Furthermore, the DUB Rpn11 (green) shifts to a central location, occluding the processing pore. The extra density (red) observed in the reconstruction of the degrading proteasome is attributed to a globular domain of the substrate.

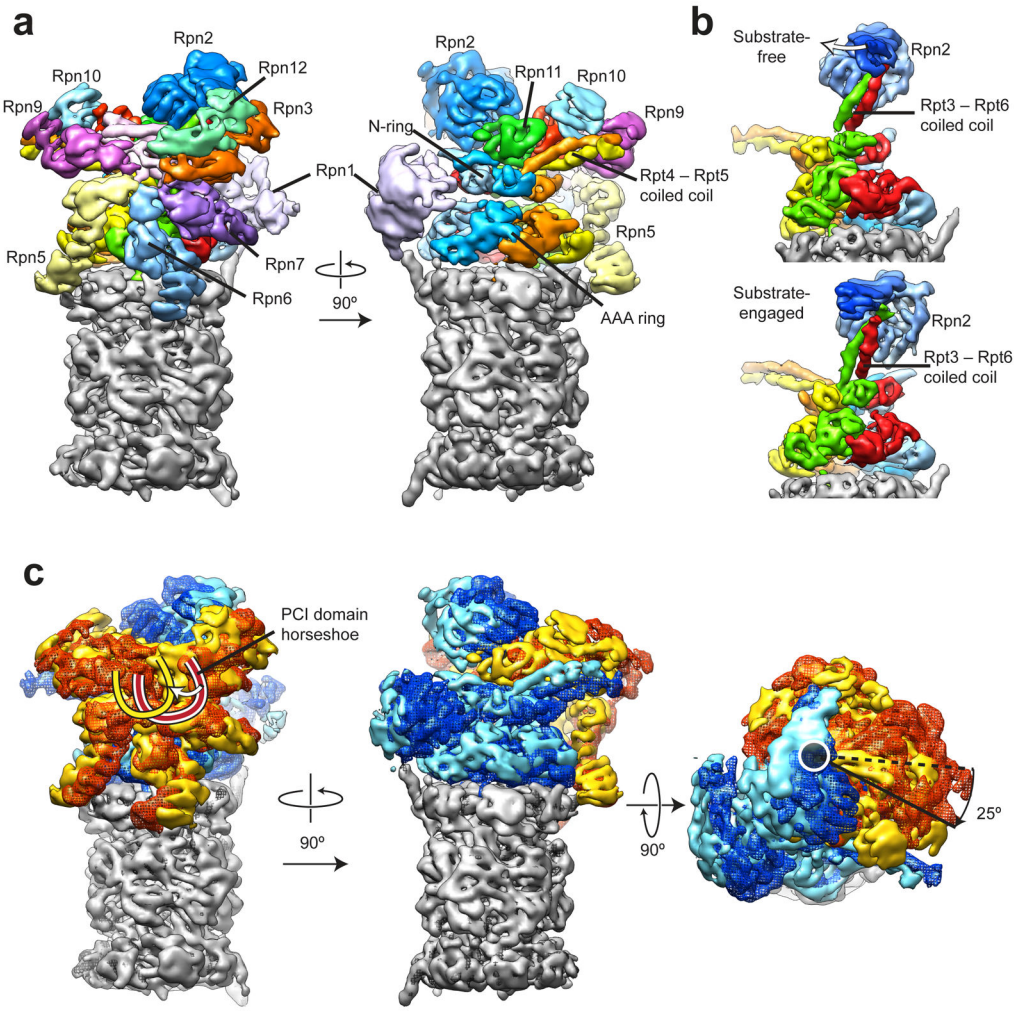

Figure 2. The subnanometer-resolution structure of the substrate-engaged 26S proteasome

(**a**) The segmented cryo-EM reconstruction of the substrate-engaged proteasome (Rpn11^{AXA} Rpn13Δ), with the regulatory particle colored by subunit and the peptidase in grey. (**b**) Side views of the base subcomplex in the substrate-free (top) and substrate-bound state (bottom), emphasizing the substrate-induced twisting of the Rpt3–Rpt6 coiled coil (green/red) that results in a rotation of Rpn2 (blue). The core-particle densities were aligned for this comparison. (**c**) The motions associated with substrate engagement are depicted by overlaying the substrate-free and substrate-bound structures that are aligned by their 20S peptidases. The base (apo as blue mesh, substrate-bound as solid cyan) and the lid (apo as red mesh, substrate-bound as solid yellow) undergo large rotations and shifts, while the peptidase (apo as black mesh, substrate-bound as solid grey) does not exhibit notable differences. On the left, the red and yellow curved lines illustrate the movement of the horseshoe-shaped arrangement of PCI domains from its substrate-free to substrate-bound position, respectively. On the right, a top view illustrates the 25° rotation of the upper regulatory particle around the axis of the Rpt3–Rpt6 coiled coil (black circle).

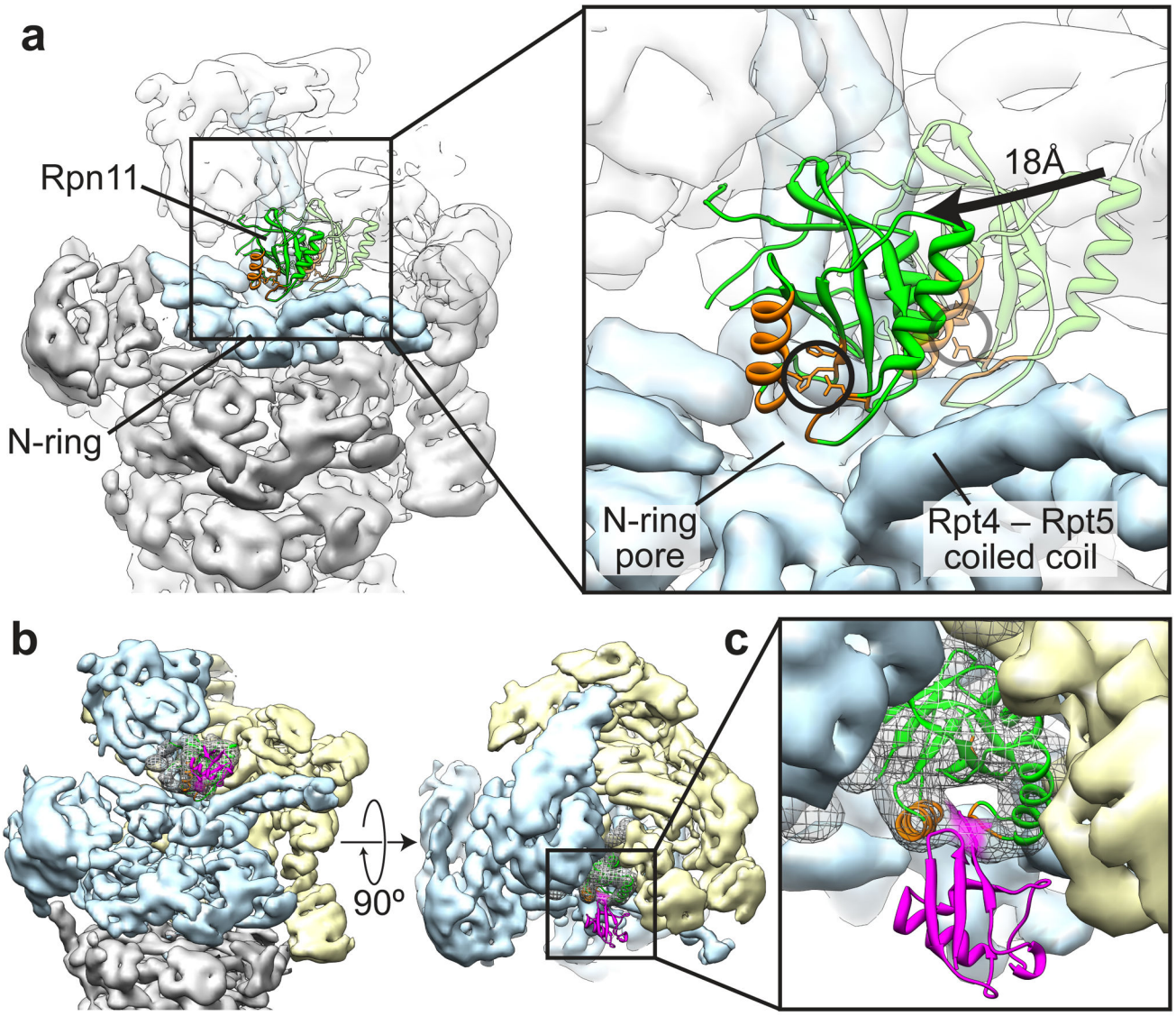

Figure 3. Rpn11 is coaxially aligned with the ATPase pore in the substrate-engaged state

(**a**) An atomic model of the DUB Rpn11 (PDB ID: 4B4T) is used to show the substrate-induced movement of this subunit relative to the N-ring. In the substrate-free state, Rpn11 (semi-transparent green ribbon), with the residues predicted to form the catalytic groove [42] highlighted in orange, is situated to the side of the N-ring and behind the Rpt4–Rpt5 coiled coil. Conformational changes in the regulatory particle shift Rpn11 to a position directly above the N-ring pore in the substrate-bound state (opaque ribbon). (**b**) The expected orientation of a ubiquitin moiety (purple ribbon)[42] with its C-terminus bound in the Rpn11 catalytic groove (Rpn11 electron density in green mesh, atomic model in green ribbon with catalytic groove highlighted in orange) is shown from a side and top view. **c,** Close-up of the modeled interactions between ubiquitin and Rpn11 from the top view. The continuous density closing the catalytic groove (purple mesh) may correspond to the C-terminus of ubiquitin.

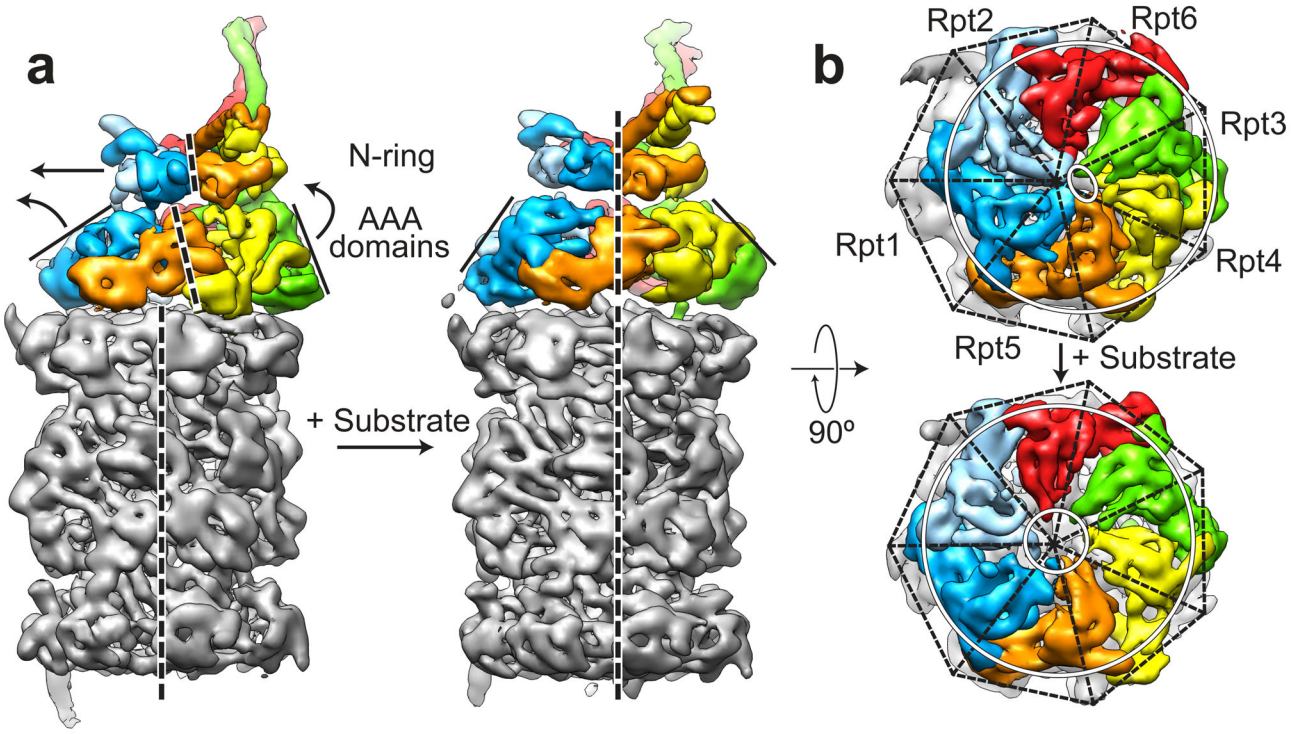

Figure 4. Substrate-induced rearrangement of the ATPase subunits creates a widened pore and a continuous central channel throughout the enzyme

(**a**) The segmented electron densities corresponding to the ATPase subunits Rpt1-Rpt6 (rainbow) and the peptidase (grey) are shown for the proteasome in the absence (left) and presence (right) of substrate, with dotted lines indicating the axes of the central channels. Substrate-engagement causes the AAA+ domains of the Rpts to individually rotate and shift into a more symmetric and coaxially-aligned ring. The N-ring also tilts and shifts, and together these changes result in the formation of a continuous channel through the ATPases to the peptidase. (**b**) The peptidase (grey) and the AAA+ domains of the ATPases (rainbow) are shown from above in the absence (top) and presence (bottom) of substrate, with dashed black lines indicating the 7-fold symmetry of the peptidase below. The large white circles encompassing the AAA+ domains emphasize the degree of alignment between the AAA+ ring and the peptidase. The smaller white circles depict the ATPase-pore diameters for the two states.

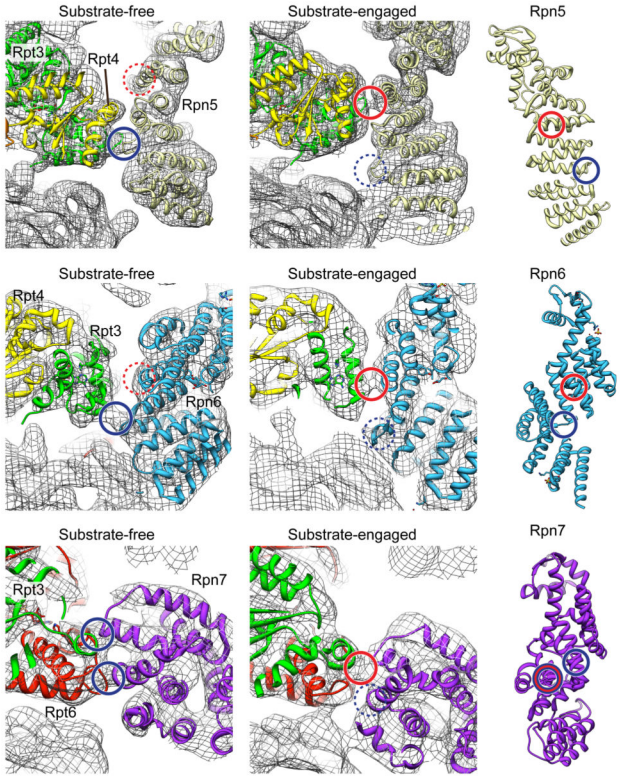

Figure 5. Bi-modal stabilization of the pre-engaged or translocation-competent base conformation by the lid

Close-up view of the lid-base interface highlights alternative contacts between Rpt and Rpn subunits in the substrate-free and substrate-engaged conformations of the regulatory particle. The positions of Rpt3 (green), Rpt4 (yellow), and Rpt6 (red) within the substrate-free and substrate-engaged EM densities (grey mesh) are shown using fitted crystal structures of the homologous PAN AAA+ domain (PDB ID: 3H4M). The crystal structure of Rpn6 (cyan, PDB ID: 3TXN [49]) and homology models of Rpn5 (PDB ID: 4B4T, light yellow) and Rpn7 (PDB ID: 4B4T, purple) [25] are shown on the right and docked into their corresponding positions in the EM density (middle and left). Both Rpn5 and Rpn6 interact with the small AAA+ subdomain of Rpt3, while Rpn7 contacts the interface between the small AAA+ subdomain of Rpt6 and the large AAA+ subdomain of Rpt3. These interactions in the substrate-free state are highlighted with solid blue circles. The substrate-engaged reconstruction reveals that Rpt3 switches its contacts with Rpn5 and Rpn6 to new binding sites (solid red circles) that are located 30 and 25 Å further toward the respective PCI domains. In contrast, Rpn7 remains in contact with the Rpt6/3 interface, but reduces its interaction points from two (blue circles) to one (red circle). This semi-static joint with Rpn7 may function as a pivot point in switching from a substrate-free to a substrate-bound conformation of the regulatory particle. Dashed circles indicate the corresponding contacts in the alternative conformation.

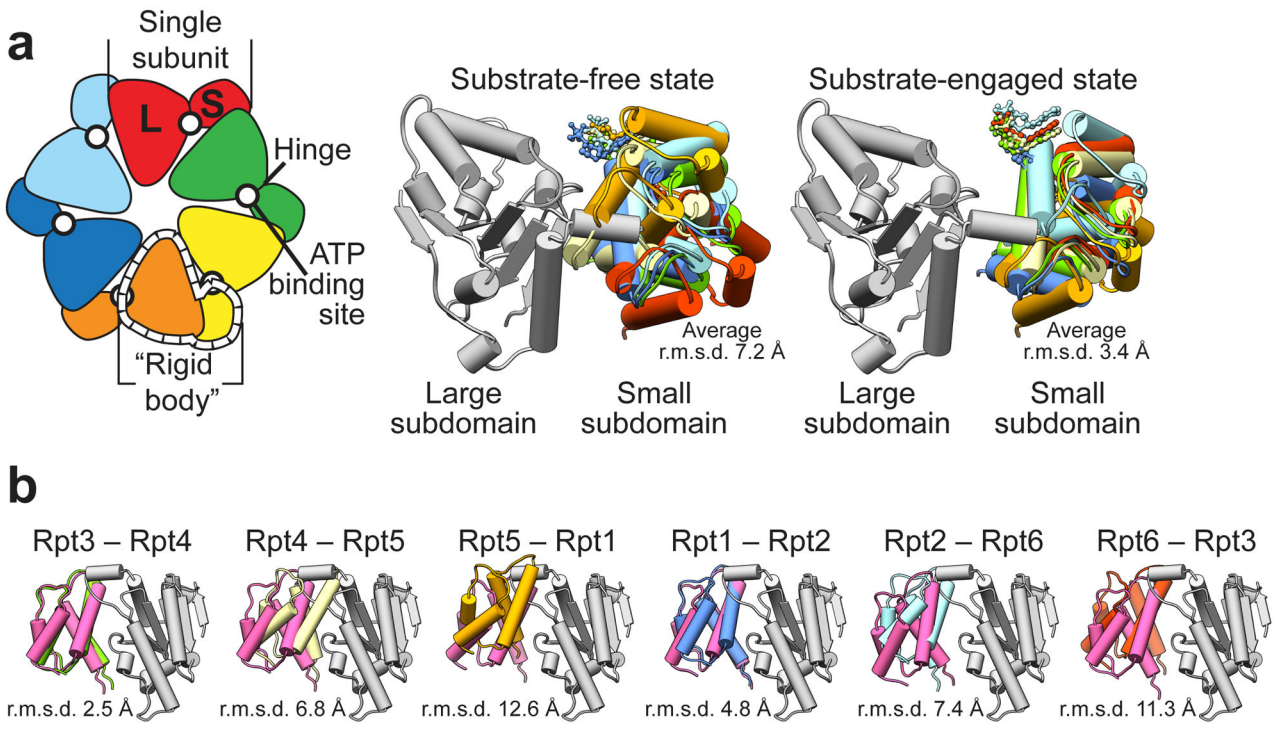

Figure 6. The translocation-competent conformation of the base exhibits uniform AAA+ domain interfaces

(**a**) On the left, a cartoon with subunits individually colored delineates the inter-subunit "rigid body" (dashed line) formed from a small AAA+ subdomain and the large AAA+ subdomain of its counterclockwise neighbor [43,44]. The six "rigid bodies" derived from docked crystal structures of individual large and small AAA+ subdomains of the homologous PAN (PDB ID: 3H4M) were superimposed by aligning the large subdomains. Substrate engagement induces uniform interfaces between subdomains of neighboring subunits, reflected by a lower average RMSD of the small subdomains. (**b**) "Rigid bodies" formed between large and small AAA+ subdomains at each Rpt interface in the absence and presence of substrate are superimposed and aligned by their large subdomain (grey). The small AAA+ domains are shown individually colored in the substrate-free state and magenta in the bound state.

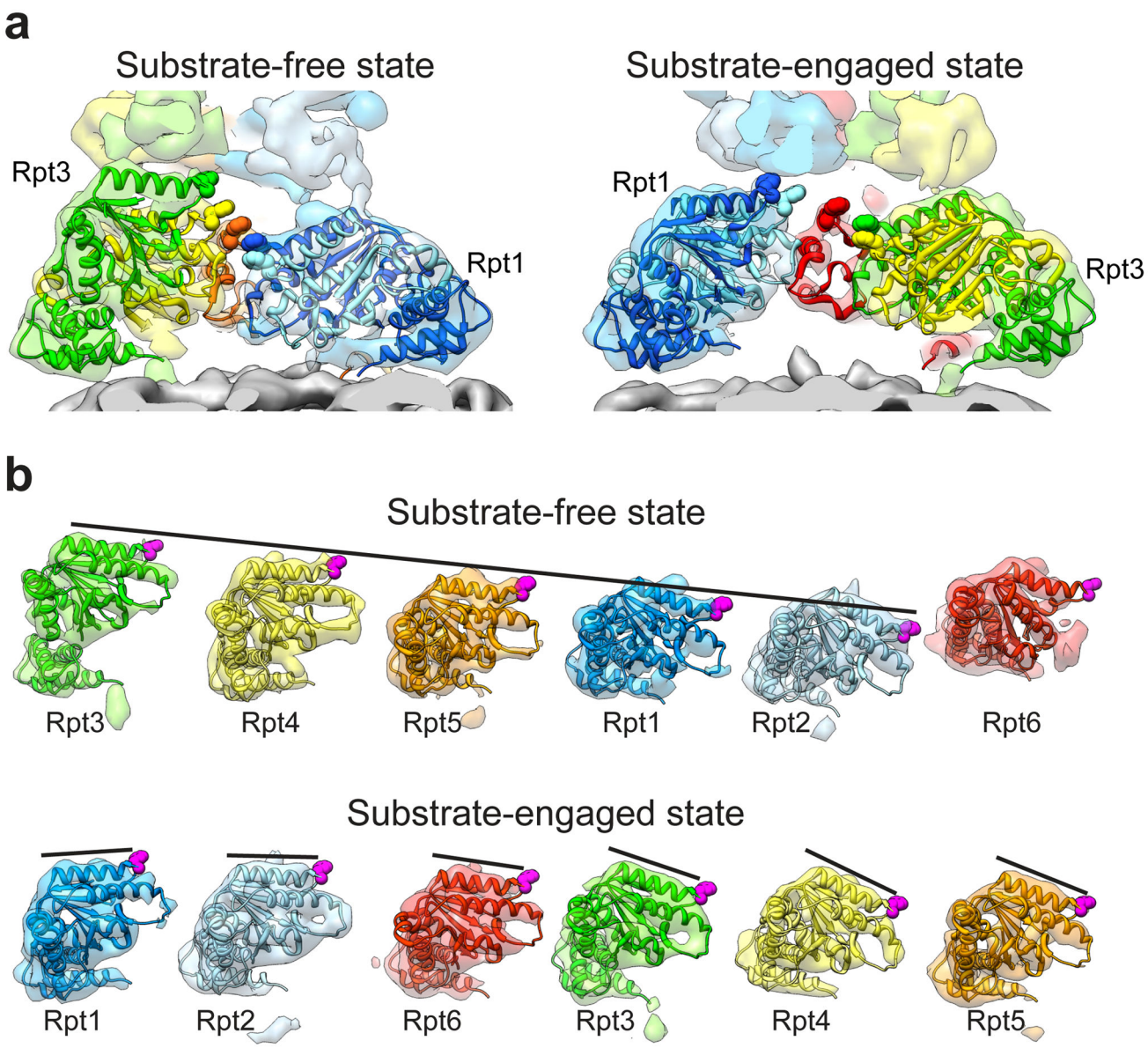

Figure 7. Rearrangement of the spiral staircase upon substrate engagement

(**a**) Cutaway side view of the Rpt ring in the substrate-free (left) and substrate-engaged (right) state, with Rpt6 and Rpt5 removed for clarity, respectively, and oriented with the top subunit of each spiral staircase on the left. Individually docked copies of the PAN crystal structure (ribbons, PDB ID: 3H4M) reveal different spiral staircase arrangements in the two states, which are emphasized by a sphere representation of the pore-loop residue that is predicted to drive translocation. (**b**) The AAA+ domains of Rpt1–Rpt6 are shown individually in the same orientation, with their pore loops facing right and the aromatic pore-loop residue shown in purple. In the absence of substrate, the entire AAA+ domains are rotated to varying degrees away from the central pore, leading to a pronounced spiral-staircase arrangement of large subdomains with a global pitch that is indicated by a continuous line. Substrate engagement arranges the AAA+ domains at a more uniform

height, with a lower-pitch spiral staircase of pore loops established solely through varied tilting of the large subdomains (emphasized by black lines).

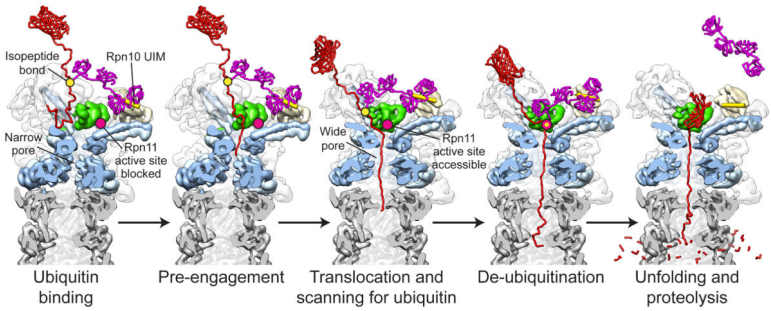

Figure 8. Structure-based model for substrate engagement and degradation by the 26S proteasome

Cutaway side view of the proteasome reconstructions in the substrate-free and engaged conformations. In the first step, substrate (red) is tethered through its ubiquitin chain (purple) to the UIM of Rpn10 (yellow cylinder). In this pre-engaged state, the flexible substrate tail can enter the accessible N-ring pore and contact the uppermost subunits of the AAA+ domain spiral staircase. Upon substrate engagement, the Rpts become rearranged into a new spiral staircase with a widened central pore that is aligned with the N-ring and subjacent peptidase (grey). Concomitantly, Rpn11 (green) shifts to a central location directly above the N-ring pore, exposing its active site (pink dot) for ubiquitin scanning along the translocating polypeptide. All ubiquitin modifications are removed as their isopeptide attachment site (yellow dot) passes by Rpn11, facilitating fast translocation, unfolding, and degradation of the substrate.